Epitaxial growth of $Co_xMn_ySi_z$ (111) thin films in the compositional range around the Heusler alloy Co_2MnSi

Liang He, Brian A. Collins, and Frank Tsui[a)]
Department of Physics and Astronomy, University of North Carolina, Chapel Hill, North Carolina 27599-3255

Yong S. Chu
National Synchrotron Light Source II, Brookhaven National Laboratory, Upton, New York 11973

(Received 5 November 2010; accepted 26 February 2011; published 18 March 2011)

Epitaxial growth and structural properties of $Co_xMn_ySi_z$ thin films on Ge (111) substrates, including the Heusler alloy Co_2MnSi (111), have been studied using combinatorial molecular beam epitaxy (MBE) techniques. *In situ* reflection high energy electron diffraction and *ex situ* x-ray diffraction experiments show that high quality coherent MBE growth with fcc (111) stacking can be achieved over a relatively large composition space that includes Co_2MnSi. The highest structural and chemical ordering is observed near the composition of $Co_{0.63}Mn_{0.14}Si_{0.23}$ rather than that at the Heusler stoichiometry of Co_2MnSi. The in-plane crystallographic axis of the fcc film exhibits a 60° rotation with respect to that of the Ge substrate. The rotation appears to be originated at the film-substrate interface, as a result of the symmetry and stacking of the Ge (111) surface reconstruction. © *2011 American Vacuum Society.* [DOI: 10.1116/1.3567419]

I. INTRODUCTION

The full Heusler alloy Co_2MnSi is among the first predicted half-metallic ferromagnetic materials with a fully spin polarized state at the Fermi level and a gap in the minority spin state.[1–3] It has a cubic crystal structure with a lattice parameter (5.654 Å) that is nearly lattice matched with standard semiconductor substrates, including Ge (5.658 Å) and GaAs (5.653 Å). Stoichiometric films and heterostructures have been successfully grown by molecular beam epitaxy (MBE). The structural compatibility with Si-based materials, when combined with its high Curie temperature (985 K) and large magnetic moment ($\sim 5\mu_B$),[4,5] and a predicted large minority spin gap (0.81 eV) (Ref. 6) make the Heusler alloy an attractive candidate as an electronic spin polarizer and filter that can potentially be integrated onto Si-based complementary metal-oxide semiconductor platform for the science and technology of spintronics. However, experiments to date on stoichiometric materials have shown rather low spin polarization, less than 60%,[7] which has been attributed to the possible presence of various structural and chemical disorders, such as site swapping between Co and Mn, antisites, and vacancies.[8–10] First-principles calculations[8–10] have predicted the likelihood of these disorders. While experimental confirmation of these is still very challenging,[11,12] the question of where the highest polarization and ordering is located in the composition space also deserves examination. The effects of epitaxial constraints and nonequilibrium synthesis conditions are of particular interest but have yet to be investigated. The difficulty lies in the large parameter space of a ternary system, but the advent of combinatorial MBE has changed that, where the dependence on composition of a complex material system can be examined systematically using one or a few samples.[13]

This article reports a systematic study of epitaxial growth and structural and chemical ordering of $Co_xMn_ySi_z$ thin films on Ge (111) substrates in the composition ranges of 30–80 at. % Co, 10–60 at. % Mn, and 10–60 at. % Si using advanced combinatorial synthesis and characterization techniques. The work is focused on the evolution of structural quality and surface morphology as a function of composition and their dependence on growth temperature. It is aimed at mapping out the epitaxial phase diagram for the ternary system and exploring the nature of epitaxy and the conditions for highest structural and chemical ordering in and around the composition of the Heusler alloy Co_2MnSi.

II. EXPERIMENT

Synthesis of the $Co_xMn_ySi_z$ thin films on Ge (111) substrates was carried out using advanced combinatorial MBE techniques.[14] A multilayer method, sequential deposition of monolayer wedges of each element, was employed for the combinatorial synthesis, as shown in Fig. 1. Each monolayer wedge was deposited across the substrate by moving a precision shadow mask, and the flux was controlled by atomic absorption spectroscopy, as detailed elsewhere.[14] Prior to the growth of each alloy film, a 200 Å Ge (111) buffer layer was grown on Ge substrate at 300 °C and annealed at 650 °C, resulting in a uniform atomically smooth Ge surface across the entire substrate with a 2×8 surface reconstruction. A multilayer sequence of Si–Co–Mn was used, which was typically repeated 200 times for each sample. Co, Si, and Ge were evaporated from e-beam hearths and Mn was evaporated from an effusion cell at a deposition rate of ~0.1 Å/s and growth pressure of $<10^{-9}$ torr. Two types of composi-

a)Author to whom correspondence should be addressed; electronic mail: ftsui@physics.unc.edu

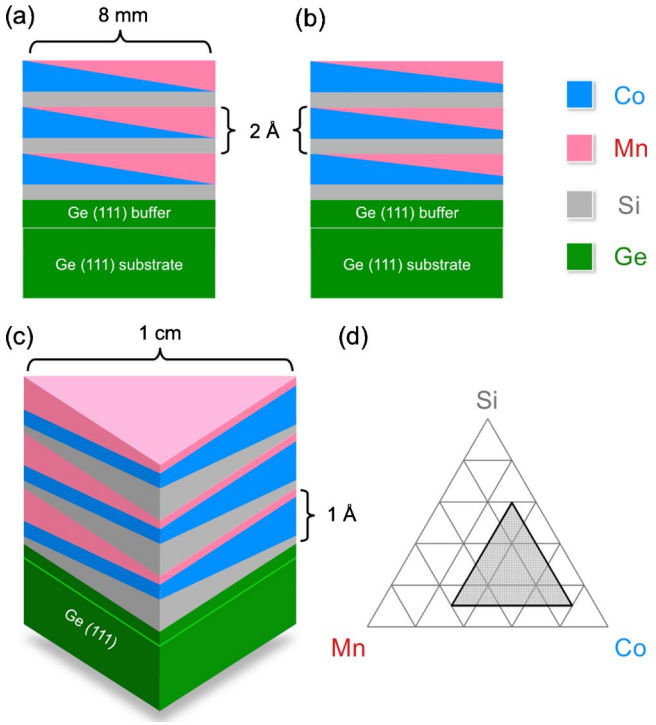

FIG. 1. (Color online) Schematic diagrams of composition spread samples. Cross-sectional view of (a) full binary sample of the type $(Co_xMn_{1-x})_aSi_{1-a}$ with $0 \le x \le 1$ and (b) partial binary sample with $0.3 \le x \le 1$. (c) Partial ternary sample and (d) composition range of the partial ternary sample (shaded region) within the full ternary phase diagram. The trilayers of Si–Co–Mn submonolayer wedges and "partial" wedges are typically repeated 200 times.

tion spread films were grown: (1) partial ternary samples of $Co_xMn_ySi_z$ with a composition range mentioned above (i.e., the ternary compositions $0.3 \le x \le 0.8$, $0.1 \le y \le 0.6$, and $0.1 \le z \le 0.6$), as shown in Figs. 1(c) and 1(d), and (2) partial binary samples of $(Co_xMn_{1-x})_{1-a}Si_a$ with x as the "binary composition," varying between 0.3 and 1 at fixed a values of 0.23, 0.25, and 0.27, as shown in Fig. 1(b). The partial composition spread samples were designed to zoom into the intended region of interest, thus enhancing composition resolution [see Fig. 1(d)]. The dependence on growth temperature between 150 and 350 °C has been examined. Results for ternary samples and binary samples grown at 150, 225, and 300 °C are presented here. Uniform samples at various compositions were also grown and examined, where the "combinatorial results" were reproduced.

Epitaxial growth of the binary samples was examined in real time by scanning reflection high energy electron diffraction (RHEED). A 30 keV RHEED beam was focused to ~50 μm in diameter, corresponding to a maximum composition spread within the beam of about 1 at. % for a full binary sample [Fig. 1(a)], and it can be scanned across the sample along a fixed crystallographic azimuth in order to probe composition dependence.[14] The incident angle of the RHEED can also be scanned by either sample rocking (tilting) or beam rocking[14] in order to examine the nature of the truncation rods. For a streaky RHEED pattern, the peak intensities along the streaks are located at the specular spots, as the Ewald sphere cuts through the truncation rods, whereas the counterparts for a spotty pattern occur at the three-dimensional (3D) Bragg reflections. For exploring surface roughness, the incident angle was adjusted with the zeroth order specular spot positioned between two zeroth order Bragg reflections, the so-called anti-Bragg position, and for this study it was approximately 2.6° with respect to the sample surface.

Composition and structure of both binary and ternary samples were studied and quantified *ex situ* using microbeam x-ray fluorescence spectroscopy (XRF) and x-ray diffraction (XRD) techniques at beamline 2-BM of the Advanced Photon Source at Argonne National Laboratory.[15] The Kirkpatrick–Baez x-ray mirrors were used to focus the beam to a spot size of ~5 μm in dimensions, resulting in a maximum composition spread within the beam of about 0.1 at. %, and the x-ray flux was about 10^9 photons/s at 10.5 keV. The composition dependence was probed by scanning the sample with respect to the x-ray spot using precision sample positioners mounted on a four-circle diffractometer. The relative uncertainties of the composition as determined by the XRF measurements are better than 3%.[16]

The full Heusler alloys crystallize in the cubic $L2_1$ structure,[2,5] which consists of four interpenetrating fcc sublattices and produces three unique families of Bragg reflections:[5] one "fundamental" {022} and two "superstructure" {002} and {111} reflections.[16,17] The fundamental reflection is insensitive to chemical disorder, being the simple sum of the atomic form factors, whereas the superstructure reflections involve differences of sublattice form factors, thus sensitive to chemical disorders. Specifically, {111} reflections are sensitive to swapping between Si and Mn, whereas {002} reflections are sensitive to that between Co and the other two elemental sites. For a random alloy, the XRD intensities at the superstructure reflections would be suppressed. Both in-plane and out-of-plane scans of these reflections were done in order to investigate various aspects of the film's crystal structure and quality.

III. RESULTS AND DISCUSSION

Under the conditions detailed above, the initial growth of $(Co_xMn_{1-x})_{1-a}Si_a$ on Ge (111) at low coverages is smooth pseudomorphic for compositions with x values between 55% and 95% and a between 0.23 and 0.27, as indicated by sharp streaky RHEED patterns. The corresponding range of Co concentrations is between 42 and 73 at. % for $a=0.23$ (i.e., 23 at. % of Si). Outside this composition range, the film is highly disordered with featureless RHEED dominated by diffused scattering. Above a thickness and composition dependent threshold, the RHEED patterns become spotty, i.e., transmission diffraction patterns, indicative of rough 3D growth, as shown in Fig. 2 at a coverage of 310 Å. The onset of the roughening transition from streaky RHEED patterns [Fig. 2(b)] to spotty patterns [Fig. 2(a)] is accompanied by an abrupt shift in the peak position of the RHEED spot [the dotted line near $x \sim 77\%$ in Fig. 2(c)]. The presence of the shift is the result of how the RHEED beam was aligned, as

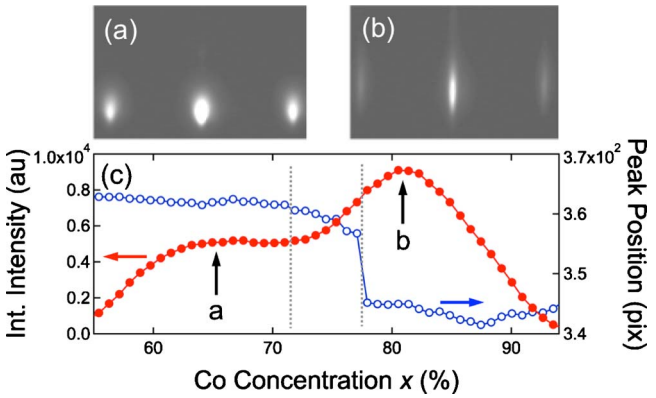

FIG. 2. (Color online) Evolution of surface structure and morphology of $(Co_xMn_{1-x})_{0.77}Si_{0.23}$ grown on Ge (111) at 225 °C and at a coverage of 310 Å. (a) and (b) Characteristic RHEED patterns along the $\langle 1\bar{1}0\rangle$ azimuth at Co concentrations of (a) 50 at. % and (b) 63 at. %. The respective binary values x are 0.65 and 0.82. The RHEED beam is aligned such that the specular reflection from the 2D streaky patterns (b) is positioned away from the Bragg reflection exhibited by the 3D transmission patterns (a) in the out-of-plane [111] direction (the down direction in the images). (c) Composition dependence of integrated RHEED intensity (close circles) and peak position (open circles) of the zeroth order spot along the out-of-plane [111] direction. The labels indicate the respective RHEED patterns shown in (a) and (b). The dotted lines indicate the roughening transitions discussed in the text.

described above. As x decreases from the abrupt transition, the slightly elongated RHEED spots become narrower and the peak position shifts toward the Bragg spot, indicating the presence of a more subtle transition from a smoother 3D surface to a rougher one [the dotted line near $x\sim72\%$ in Fig. 2(c)]. At this coverage of 310 Å, the film is rough near the Heusler stoichiometry (x around 65%), whereas a Co-rich region (x around 82%) of the film exhibits the best surface quality with the highest RHEED intensity and narrowest in-plane width.

The evolution of the thickness and composition dependent roughening transition has been examined by tracking the RHEED intensity and peak position. As shown in Fig. 3(a), smooth two-dimensional (2D) growth proceeds up to a critical thickness, where a transition to 3D rough growth occurs. As described above, the roughening transition undergoes an abrupt one [close symbols in Fig. 3(a)] from streaky RHEED patterns to elongated spotty patterns and followed by a subtle transition [open symbols in Fig. 3(a)] from a smoother 3D surface (elongated spots) to a rougher one (spots). Up to 100 Å, the RHEED intensity is the highest near the Heusler stoichiometry with binary concentration $x\sim70\%$ indicating the highest quality surface. With increasing thickness, however, the highest intensities shift to $x\sim80\%$. The trend follows the behavior of the roughening transition, where 3D RHEED patterns appear just above 100 Å at $x\sim55\%$ and gradually expand toward higher Co concentration with increasing thickness [the lines and points in Fig. 3(a)]. The observed behavior seems to take on some characteristics of critical thickness for lattice relaxation, but as described below, the alloy film is either lattice matched or nearly matched with that of Ge and it stays coherent in plane for x between 65% and 90%. In other words, lattice relaxation is not the mechanism for the behavior. At different growth temperatures between 150 and 300 °C, the samples exhibit the same qualitative thickness dependent behavior, as shown in Fig. 3(b). Quantitatively, samples grown at 225 °C exhibit the largest 2D region (the smallest 3D region) in composition when these are compared to the counterparts grown at temperatures above and below.

The epitaxial phase diagram of the ternary system has been examined using ternary combinatorial samples, as shown in Fig. 4. XRD experiments reveal that high quality coherent MBE growth with fcc stacking can be achieved over a relatively large composition space, region 1 in Fig. 4(a). There are two additional distinct regions, where the film exhibits either a mixture of two phases in region 2 or disordered nanocrystalline phase in region 3. In Fig. 4(b), XRD intensity profiles along an out-of-plane off specular direction (i.e., [01L] scans in hexagonal notation[15]) illustrate the different structures in the three distinct compositional regions. The reflection at $L=5$ seen in all three profiles is the diamond (113) reflection from the substrate. Also present in all the profiles is the reflection at $L=2$, which is identified as stacking faults within the substrate.

The cubic fcc structure [open circles in Fig. 4(b)] has reflections at $L=1$ and 4, corresponding to the cubic (111) and (022), respectively, with peak intensities that are more than one order of magnitude higher than any other phase in the ternary sample. The two reflections of the film are rotated 60° from the corresponding ones of the substrate.[15–17] At the substrate reflections, while more difficult to detect owing to

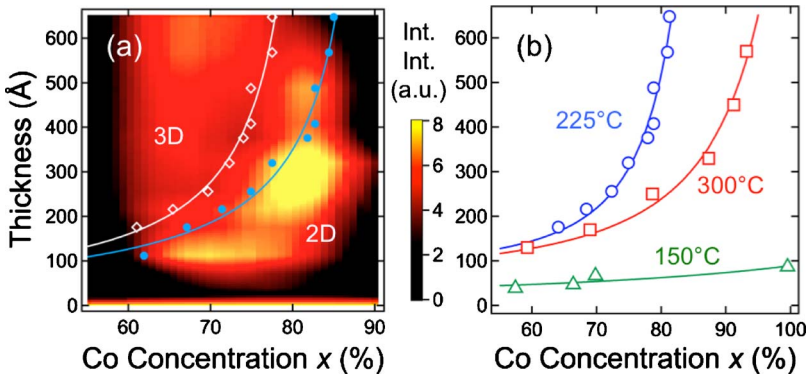

FIG. 3. (Color online) Evolution of the surface morphology for $(Co_xMn_{1-x})_{0.77}Si_{0.23}$. (a) Image of integrated RHEED intensity and graph of roughening transition (symbols and lines) vs binary concentration and coverage for growth at 225 °C. The close and open symbols correspond to the abrupt roughening transition and the subtle transition from smoother quasi-3D surface to rougher 3D surface, respectively [the two dotted lines in Fig. 2(c)]. (b) Roughening transition at three growth temperatures of 150 (triangles), 225 (circles), and 300 °C (squares). The points correspond to the midpoints between the two transition points at the same coverages. The solid lines are guide for the eyes.

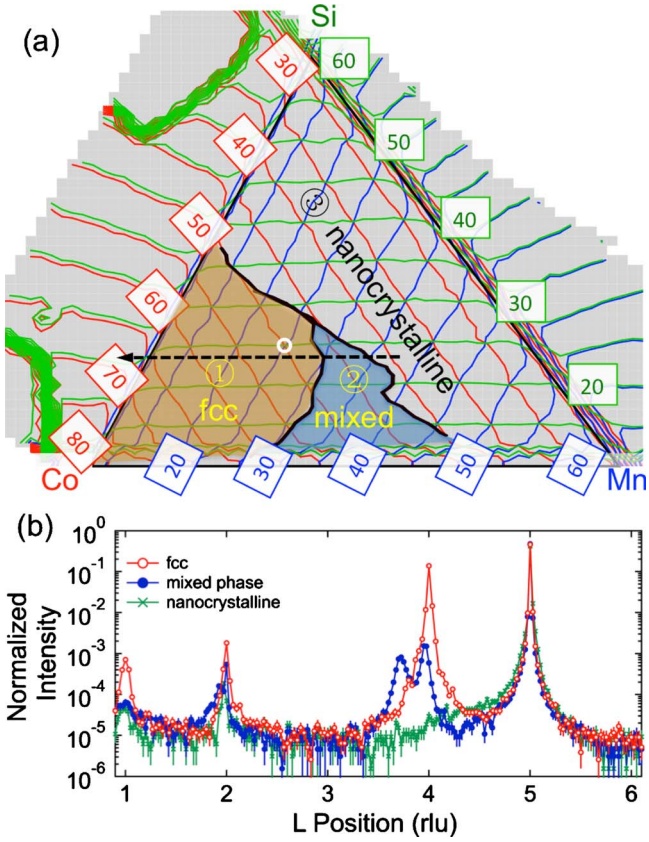

FIG. 4. (Color online) Epitaxial phase diagram of a ternary combinatorial film $Co_xMn_ySi_z$ grown on Ge (111) at 300 °C. The nominal film thickness is 370 Å. (a) Crystallographic phases vs composition, where thick black lines delineate three distinct regions, (1) cubic fcc, (2) mixed cubic and hexagonal, and (3) disordered nanocrystalline. The concentration contours that correspond to the concentrations of Co, Mn, and Si, respectively, were obtained from XRF measurements. The white circle within the fcc region indicates the composition of the Si Heusler. The horizontal dashed line indicates the approximate compositions for the binary samples, whereas the arrow on the left denotes the direction of x shown in Figs. 2, 3, and 6. (b) Characteristic out-of-plane off-axis XRD scans along [01L] [in hexagonal notation (Ref. 15)] from each of the regions, fcc (open circles), mixed phase (close circles), and nanocrystalline (crosses). The respective XRD scans were taken at compositions of $Co_{0.54}Mn_{0.20}Si_{0.26}$, $Co_{0.44}Mn_{0.38}Si_{0.18}$, and $Co_{0.38}Mn_{0.28}Si_{0.34}$. The peak at L=5 is from the Ge substrate.

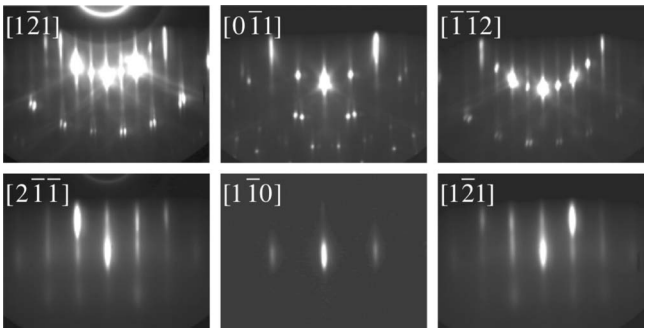

FIG. 5. Threefold symmetry of RHEED patterns for fcc (111) surface. Top row: RHEED patterns of the Ge (111) surface along various azimuths; bottom row: those of the Heusler alloy along the same respective azimuths of the Ge. The direction labels in the bottom images are indexed with respect to the crystal structure of the alloy.

the high intensity from the substrate, the reflections from the films are undetectable. These observations indicate that the high quality fcc film consists of a single domain and its crystallographic axis is rotated by 60° in the growth plane with respect to that of the Ge substrate. For example, the in-plane [1$\bar{1}$0] of the film is parallel to the [0$\bar{1}$1] of the substrate.

The intensity profiles associated with the mixed phase [close circles in Fig. 4(b)] show a broad low intensity fcc phase with a peak at L=3.96, which is accompanied by a broader intensity at L=3.73, evidently from a disordered hexagonal phase [hexagonal (012) reflection]. The presence of a broad peak, a shoulder near L=1.87 [hexagonal (012)], supports the assessment that the second phase is hexagonal. Owing to disorder, the intensity from the hexagonal (013) (L=5.60) is expected to be below the detection level of the scan with modest data integration time. In the Mn- and Si-rich regions of composition, only diffused intensities were detected. Again, the intensity from disordered nanocrystals is weak and below the detection level. The nanocrystalline phase is likely due to the presence of a large variety of Mn silicides that suppresses epitaxial growth and formation of large crystalline grains.

RHEED analysis supports the above observation that the film exhibits a 60° rotation with respect to the substrate. As shown in the bottom row of Fig. 5, the RHEED patterns from the film exhibit threefold symmetry, particularly for {112} azimuths, where the modulated quasi-2D patterns show asymmetry with respect to the zeroth order reflection. The onset of the asymmetric patterns is determined to be during the deposition of the first two atomic layers of the alloy. This observation suggests that the 60° rotation is originated at the alloy-Ge (or film-buffer layer) interface. One likely explanation is the presence of a single stacking fault at the interface, as a result of the Ge 2×8 surface reconstruction. In the 2×8 structure, the atoms in the topmost adatom layer are located directly above those in the second layer below, the so-called "on-top site,"[18] while all the surface and near surface layers, except the adatom layer, are bulklike. Therefore, the topmost layer in the 2×8 structure is equivalent to a stacking fault, and the stacking for the Heusler alloy is perhaps initiated here. We note that cubic (111) films of $Co_xMn_yGe_z$ alloys also exhibit the same 60° rotation.[15–17]

Further XRD analysis has been carried out with the results shown in Fig. 6. The composition dependence of the fundamental intensity [open circles in Fig. 6(a)] exhibits a peak at the Heusler stoichiometry (x~69%) and a higher peak at x~85%, indicating high structural ordering at these compositions. This finding is consistent with the RHEED analysis, where the integrated RHEED intensities exhibit a peak near the latter compositions [Fig. 2(c)]. The intensities at the superstructure reflections [(002) and (111), diamonds and close circles in Fig. 6(a)] also show high values in the same composition range, with the highest intensities at x~78%, indicating the highest chemical ordering. Correspondingly, the coherence lengths are the longest, as indicated by the narrow full width at half maximum (FWHM) of

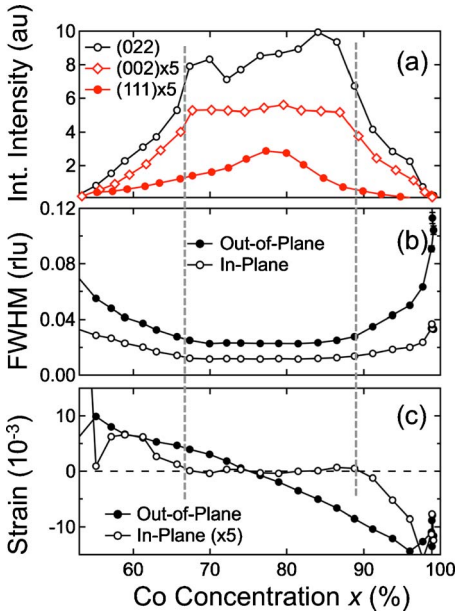

FIG. 6. (Color online) Composition dependent XRD analysis of $(Co_xMn_{1-x})_{0.77}Si_{0.23}$ grown at 300 °C and 540 Å thick. (a) Integrated intensities along the out-of-plane direction of (022), (002), and (111) cubic reflections. The intensities for the latter two superstructure reflections are multiplied by 5. (b) In-plane and out-of-plane FWHMs of the fundamental (022) reflection. (c) In-plane and out-of-plane strains with respect the substrate. For clarity, the in-plane strain is multiplied by 5. The vertical dashed lines indicate the region with zero in-plane strain (coherent growth). The scatter in the points at Co concentration below 55% and above 95% is the result of low diffraction intensity (polycrystalline regions).

the XRD peaks [Fig. 6(b)]. The shorter out-of-plane crystalline coherence length (broader FWHM), as compared to the in-plane counterpart, is limited by the film thickness. The in-plane strain values [Fig. 6(c)] confirm that the film is epitaxially coherent within the highly ordered region of composition, while the out-of-plane counterpart is linear and thus obeys Vegard's law. At $x \sim 75\%$, the alloy film is lattice matched with Ge. It is interesting to note that the highest (022) intensity is at a different concentration, as mentioned above. Samples grown at different temperatures show qualitatively the same composition dependence, and the highest structural and surface quality is observed for growth at 225 °C, consistent with the RHEED analysis.

The highest structural and chemical ordering is observed near the composition of $Co_{0.62}Mn_{0.15}Si_{0.23}$ rather than the Heusler stoichiometry. This composition appears to be growth temperature invariant, indicating the important role played by energetics. However, the cause for the observed shift in the most ordered composition and the thickness dependence is unclear. This question and others such as the mechanism for the observed rough growth in the absence of strain await further investigations.

IV. SUMMARY

MBE growth and structural and chemical ordering of $Co_xMn_ySi_z$ thin films on Ge (111) substrates have been investigated, including the full Heusler alloy Co_2MnSi. Coherent epitaxy of fcc structure can be achieved over a large region of composition. Alloy film is a 60° twin of the substrate that appears to initiate at the alloy-Ge interface. The highest crystalline quality and chemical ordering is observed near a composition of $Co_{0.62}Mn_{0.15}Si_{0.23}$ rather than the Heusler stoichiometry, with the former exhibiting a slightly smaller lattice mismatch with Ge than that of the latter. The work calls for systematic investigations of spin dependent properties that include the off-stoichiometric compositions.

ACKNOWLEDGMENTS

The work was supported by DOE BES Grant No. DE-FG02-05ER46216. The use of the Advanced Photon Source was supported by DOE BES Grant No. DE-AC02-06CH11357. A part of the work was supported by the Brookhaven Science Associates, LLC under Contract No. DE-AC02-98CH10886 with the U.S. Department of Energy.

[1]R. A. de Groot, F. M. Mueller, P. G. V. Engen, and K. H. J. Buschow, Phys. Rev. Lett. **50**, 2024 (1983).
[2]S. Ishida, T. Masaki, S. Fujii, and S. Asano, Physica B **245**, 1 (1998).
[3]M. I. Katsnelson, V. Y. Irkhin, L. Chioncel, A. I. Lichtenstein, and R. A. de Groot, Rev. Mod. Phys. **80**, 315 (2008).
[4]P. J. Webster and K. R. A. Ziebeck, in *Magnetic Properties of Metals*, Landolt-Börnstein, New Series, Group III, Vol. 19c, edited by O. Madelung (Springer, Berlin, 1988), pp. 75–79.
[5]P. J. Webster, J. Phys. Chem. Solids **32**, 1221 (1971).
[6]S. Picozzi, A. Continenza, and A. J. Freeman, Phys. Rev. B **66**, 094421 (2002).
[7]L. Ritchie *et al.*, Phys. Rev. B **68**, 104430 (2003).
[8]D. Orgassa, H. Fujiwara, T. C. Schulthess, and W. H. Butler, Phys. Rev. B **60**, 13237 (1999).
[9]D. Orgassa, H. Fujiwara, T. C. Schulthess, and W. H. Butler, J. Appl. Phys. **87**, 5870 (2000).
[10]S. Picozzi, A. Continenza, and A. J. Freeman, Phys. Rev. B **69**, 094423 (2004).
[11]B. Ravel, M. P. Raphael, V. G. Harris, and Q. Huang, Phys. Rev. B **65**, 184431 (2002).
[12]M. P. Raphael *et al.*, Phys. Rev. B **66**, 104429 (2002).
[13]Y. K. Yoo and F. Tsui, MRS Bull. **27**, 316 (2002).
[14]F. Tsui and L. He, Rev. Sci. Instrum. **76**, 062206 (2005).
[15]Y. S. Chu, A. Tkachuk, S. Vogt, P. Ilinski, D. A. Walko, D. C. Mancini, E. M. Dufresne, L. He, and F. Tsui, Appl. Surf. Sci. **223**, 175 (2004).
[16]B. A. Collins, Ph.D. thesis, University of North Carolina at Chapel Hill, 2009.
[17]B. A. Collins, Y. Zhong, Y. S. Chu, L. He, and F. Tsui, J. Vac. Sci. Technol. B **25**, 999 (2007).
[18]J. Aarts, A. J. Hoeven, and P. K. Larsen, Phys. Rev. B **38**, 3925 (1988).